Rev. Cub. Física vol.25 No.2-A (2008) p.75-80
ISSN: 0253-9268. Original paper

Abril 17-19, La Habana

Revista Cubana de Física
Calle I No. 302 e/ 15 y 17
Vedado, La Habana.
www.fisica.uh.cu/biblioteca/revcubfi/index.htm

Recent advances in silicon microphotonic devices

P. Cheben, A. Delâge, A. Densmore, S. Janz, B. Lamontagne, J. Lapointe, E. Post, J. Schmid, P. Waldron, and D.-X. Xu

Institute for Microstructural Sciences, National Research Council Canada, Ottawa, Canada; pavel.cheben@nrc.ca

Recibido el 1/02/2008. Aprobado en versión final el 4/07/08.

Sumario. Se revisan diversos dispositivos de guías de onda silicon-sobre-aislante (SOI) desarrollados en el National Research Council de Canadá. Incluyen un espectrómetro de alta resolución basado en un arreglo de rejilla de guía de onda (AWG), un espectrómetro de transformada de Fourier AWG con una gran capacidad de recolección de luz y un AWG con dispersión incrementada utilizando el efecto fotónico de gap de banda. Se introducen las estructuras de rejilla sub-longitud de onda (SWG), incluyendo acopladores de entrada y caras de guía de onda antireflectantes.

Abstract: Various microphotonic silicon-on-insulator (SOI) waveguide devices developed at the National Research Council of Canada are reviewed. These include a high-resolution arrayed waveguide grating (AWG) spectrometer, a Fourier-transform interleaved AWG spectrometer with a large light gathering capability, and an AWG with the dispersion enhancement using the photonic bandgap effect. Sub-wavelength grating (SWG) structures are introduced, including input couplers and antireflective waveguide facets.

Keywords. Nonlinear waveguides, optical, 42.65.Wi, Visible and ultraviolet spectrometers, 07.60.Rd, Optical waveguides, 42.82.Et

1 Introduction

Silicon has been the dominant platform for the microelectronics industry for several decades and it appears that it will remain so in the foreseeable future. The benefit of integration of the mainstream microelectronic technology with photonics has been the main driving force in the emerging field of silicon photonics. In intrinsic single crystal silicon, light with wavelength longer than the Si bandgap wavelength (λ_g = 1.107 μm) can propagates with a low loss. Particularly attractive is the high refractive index of Si, with n ~ 3.5 at 1.55 μm. When silicon is used as the waveguide core and is surrounded, for example, by a SiO_2 cladding of n ~ 1.5, an index step of Δn ~ 2 is obtained. In such waveguides, light is highly confined in the core which can have cross-sections as small as ~ 250 nm and bending radii can be reduced to a few micrometers. Ultra-compact planar waveguide devices can hence be made in Si. In this paper, various silicon photonic devices developed at NRC Canada are reviewed.

2 High resolution AWG spectrometer

Waveguide spectrometers, including waveguide echelle gratings and arrayed waveguide gratings (AWGs)[1], perform functions such as WDM multiplexing and demultiplexing, wavelength filtering, signal routing and cross-connects, among others. New applications of spectrometer chips are emerging in optical interconnects, spectroscopy, metrology, chemical and biological sensing, medical instrumentation, and space-based sensing. Compact waveguide spectrometer chips can potentially be made with many channels and a high spectral resolution by us-

ing waveguide platforms with high index contrast, such as silicon-on-insulator.

The wavelength resolution of a bulk optic grating spectrometer (or monochromator) is determined, for a given grating and imaging optics, by the input and output slit widths. By narrowing the slit width, the resolution is improved. In an AWG spectrometer, the input and output waveguide mode size at the combiner focal planes plays the analogous role to the slit width, but this mode size is limited to several micrometers in glass waveguide AWGs. The mode size and coupling between closely spaced waveguides also limits the maximum number of channels. In silicon however, well confined single mode waveguides, or photonic wires, can be fabricated with dimensions as small as 0.2 μm. This suggests that by adopting photonic wire technology into AWG design, compact spectrometers with extremely high resolution and channel count can be fabricated[2,3].

The input waveguides and arrayed grating waveguides are conventional partially etched ridge waveguides. However, near the Rowland circles, the ridge waveguide are adiabatically transformed down to 0.6 μm wide slit waveguides deep etched down to the buried oxide. The ridge waveguides and two-level adiabatic mode converters shown in Fig. 1b are fabricated using a self-aligned two-step e-beam patterning and plasma etching process.

Fig. 2 shows the measured spectra. The adjacent and non-adjacent crosstalk is 10 dB or better. The measured channel spacing is 2 Å (25 GHz at 1550 nm), allowing to resolve spectral lines separated by ~1 Å. The waveguide scattering loss (~15 dB) is the largest contribution to the insertion loss, and the probable cause of the relatively high cross-talk. Both will be improved as our unique two-level fabrication process is optimized. This is the highest resolution reported up to date for an SOI AWG. The size advantage of this device is obvious. Previously reported 25-GHz silica AWG occupies a 4-inch wafer[4], two orders of magnitude larger than the 8x8 mm^2 footprint of our spectrometer.

3 Fourier-transform AWG spectrometer

The need for narrow input waveguide apertures to achieve a high resolution can be avoided by arranging the AWG in a Michelson configuration, which allows for a wider input aperture, a property known as *étendue* (light gathering capability or light throughput) advantage. To explore this benefit, we proposed a Fourier transform waveguide spectrometer[5] using two interleaved reflective AWGs in a Michelson configuration, as shown in Fig 3a. Light emerging from an input waveguide (IW) of width w is coupled through a slab waveguide combiner (SWC) into two interleaved reflective arrayed waveguide gratings AWG_1 and AWG_2 of interference orders m and $-m$, respectively. By interleaving the two AWGs, beam splitting and combining are achieved in a simple way (wavefront sharing), eliminating the need for a dedicated beam splitter/combiner element. The light propagates through each individual waveguide towards the truncation mirrors that reverse the light propagation direction. As the wavelength changes away from the Littrow wavelength, the two wavefronts originating from the waveguide arrays AWG_1 and AWG_2 tilt in the opposite direction according to the AWG dispersion relation. This results in Fizeau interference fringes with a wavelength-dependent period in the slab waveguide combiner where the two wavefronts overlap.

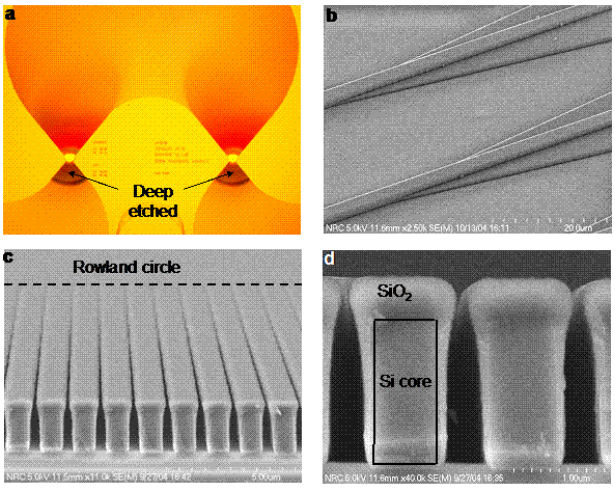

Figure 1. a) A microphotograph of a 50-channel SOI AWG spectrometer; b) SEM image of a ridge SOI waveguide adiabatically transformed into a deep-etch rectangular waveguide before joining a slab waveguide at the Rowland circle; c) Deep etched waveguides near the Rowland circle; d) detail of (c).

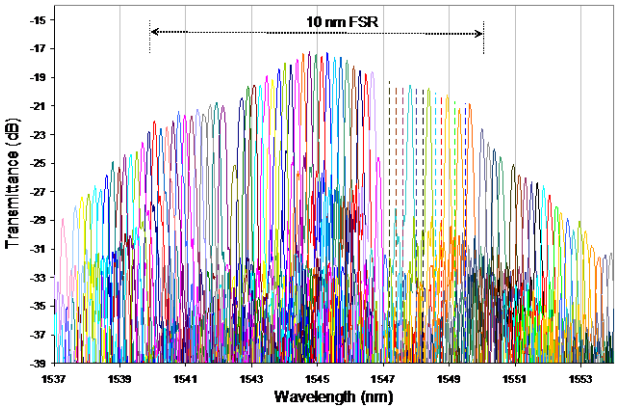

Figure 2. Measured spectra of SOI AWG spectrometer.

The interference fringes are brought to a convenient location (image curve, IC) by imaging optics (mirror, M), where the interferogram $I(x)$ is sampled by receiver waveguides (RW). Monochromatic light of wavelength λ produces a sinusoidal interferogram, whereas for arbitrary input spectral distribution $B(\lambda)$, the spectrum $B(\lambda)$ can be retrieved by Fourier transformation of the interferogram $I(x)$.

A Fourier transform AWG device has been designed for the silicon-on-insulator (SOI) platform. Fig. 3b

shows the simulated interferogram (top) for an input waveguide of width w = 40 μm, and the spectra (bottom) obtained by Fourier transformation of the interferogram. The two peaks near 1510 nm, which are separated by 0.1 nm, are well resolved for this large waveguide aperture. This is a significant increase in the aperture size compared to the grating based microspectrometers, as the latter would require, for a similar resolution and interference order, an input waveguide width of ~1 μm. There are two important advantages of this new type of device. First, as a Michelson-type interferometer it allows a larger input aperture size as compared to diffraction grating based instruments, providing an increased light throughput. Second, unlike most of the state-of-the-art FT spectrometers that require scanning mirrors, our FT AWG is a static device and gives a spectral resolution equivalent to a conventional FT spectrometer with a mirror scanning range of ~10 mm. This scanning range cannot be achieved with the current MEMS technology.

4 AWG dispersion enhancement

The AWG dispersion and resolution can be increased by modifying the group index of the waveguide array[6]. When the waveguide group index is modified within the triangular region of the waveguide array (Fig. 4a), the AWG dispersion equation becomes:

$$\sin\theta = \frac{(\lambda-\lambda_c)(M+M')}{n_{eff,s}\Lambda} = \frac{(\lambda-\lambda_c)(n_g\Delta L + \Delta n_g \Delta L_g)}{\lambda_c n_{eff,s}\Lambda} \quad (1)$$

where $M = mn_g/n_{eff}$ is the interference order of a conventional AWG with length increment ΔL between the adjacent waveguides, $M' = m\Delta n_g/\Delta n_{eff}$ is the interference order enhancement factor due to group index modification, ΔL_g is the length difference between the adjacent waveguides in the triangular section (Fig. 4a) with modified group index, and Δn_g and Δn_{eff} are respective differences in group and effective indices between the modified and unmodified waveguide sections. The index s in Eq. (1) refers to the slab waveguide combiner.

Very large Δn_g and hence a large dispersion enhancement can be obtained over a limited wavelength range near the edge of the stop band of various structures, including gratings, resonators, or photonic crystals. A 300-fold increase in group index has been reported by Vlasov et al. in SOI photonic crystal waveguides[7]. Fig. 4b shows the calculated dispersion enhancement effect for an SOI AWG[6] using the group index measurement by Notomi et al. [8].

5 Subwavelength grating fiber-chip coupler

A major problem in the design and fabrication of integrated microphotonic devices is the efficient coupling between compact planar waveguides and the input/output ports. Various original coupling solutions have been found, but the coupling still remains a challenge for waveguides of sub-micrometer dimensions made in high index contrast (HIC) waveguide platforms. Due to the large mode effective index and mode size disparities, the optical coupling between an optical fiber and a high index contrast waveguide with a small cross-section is largely inefficient. Mode size transforming structures in both the in-plane and out-of-plane directions need to be used.

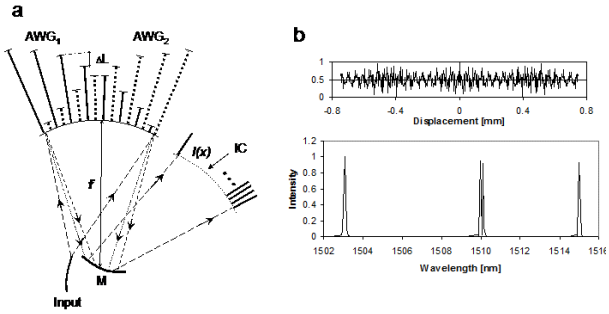

Figure 3. a) FT Michelson-type spectrometer with two interleaved reflective AWGs; b) The interferogram (top) and the calculated spectra (bottom). The light source comprises four monochromatic lines at wavelengths of 1503 nm, 1510 nm, 1510.1 nm, and 1515 nm.

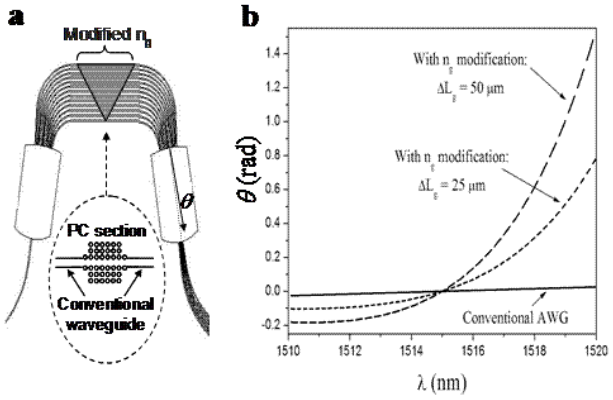

Figure 4. a) AWG with a triangular dispersion enhancing region with large group index; b) Dispersion enhancement calculated for a triangular region with photonic crystal (PC) waveguides as indicated in (a).

We have proposed a new method to couple light between an optical fiber and a planar waveguide circuit using a subwavelength grating (SWG) [9]. According to the homogenization theory or effective-medium theory, a composite medium comprising different materials combined at subwavelength scale ($\Lambda < \lambda$) can be approximated as a homogeneous media and its effective index can be expressed as a power series of the homogenization parameter $\chi = \Lambda/\lambda$, where Λ is the grating period (pitch) and λ is the wavelength of light. The coupler principle is based on gradual modification of the waveguide mode effective index by the SWG effect. A general schematic of the proposed coupling method is shown in Fig. 5.

The waveguide mode effective index is altered by chirping the SWG duty ratio $r(z) = a(z)/\Lambda(z)$, where $a(z)$

is the length of the waveguide core segment. In a general case both Λ and a may vary along the propagation direction z, but here we consider a simple case of constant Λ, as varying $a(z)$ suffices to explain the SWG effect. The effective index of the mode in the SWG coupling structures increases with the grating duty ratio. The duty ratio and hence the volume fraction of the waveguide core material is modified such that at one end of the coupler the effective index is matched to the HIC waveguide while at the other end, near the chip facet, it matches that of the optical fiber.

The SWG effect can also be combined with waveguide width tapering (Fig. 5c) and also with SWG segment height and etch depth variations arising from the reactive ion etching lag effect near the ends of the coupler, as schematically shown in Fig. 5a. Unlike waveguide grating couplers based on diffraction, the SWG mechanism is non-resonant, and hence intrinsically wavelength insensitive. Diffraction by the grating is frustrated provided the grating period Λ is less than the 1st order Bragg period $\Lambda_{Bragg} = \lambda/(2n_{eff})$, where n_{eff} is the mode effective index. Long-period mode converters[10] with $\Lambda > \lambda/(2n_{eff})$ can be used for mode size transformation in low index contrast waveguides such as those made in a silica-on-silicon platform, but their application in HIC waveguides is hindered by the reflection and diffraction losses incurred at the boundaries of different segments.

Applying the SWG approach in an SOI waveguide with Si core and SiO_2 cladding, an increasing portion of the Si core is removed and replaced with SiO_2 when approaching the coupler end facing the fiber, and an effective index close to that of silica glass is obtained at the fiber-chip interface. We demonstrated the proposed principle on various SWG coupling structures, using two-dimensional Finite Difference Time Domain (FDTD) calculations. The duty ratio is chirped linearly from $r_{min} = 0.1$ at the coupler end facing the fiber to $r_{max} = 1$ at the opposite end of the coupler. The coupling structures were simulated for an SOI waveguide with Si core thickness of 0.3 μm surrounded by SiO_2 cladding, with the corresponding refractive indices of n(Si) = 3.476 and $n(SiO_2) = 1.5$.

At the input side of the coupler, a continuous-wave (cw) Gaussian field with a width equivalent to the mode field diameter (MFD) of the optical fiber mode at a wavelength $\lambda = 1.55$ μm was assumed. Coupling efficiencies for a MFD = 10.4 μm (SMF-28 fiber) were calculated and also compared with MFD = 5.9 μm for a C-type high numerical aperture fiber. The SWG waveguide is positioned along the z axis. The maximum simulation window dimensions used were 50 μm (propagation direction) by 13 μm (transverse direction). The mesh size was 10 nm in both dimensions and the simulations ran for a total of 20,000 time steps each of $\Delta t = 2.2 \cdot 10^{-17}$ s. The coupler efficiency was calculated as $\eta = \Gamma P_2/P_1$, where P_1 is the input power injected at the right edge of the computation window ($z = z_1$), and P_2 is the output power crossing the output plane obtained by integrating the S_z component of the Poynting vector along the left edge of the computation window at $z = z_2$ where the coupler joins the silicon waveguide, and Γ is the power overlap integral of the calculated field at the output plane $z = z_2$ with the fundamental mode of the Si waveguide.

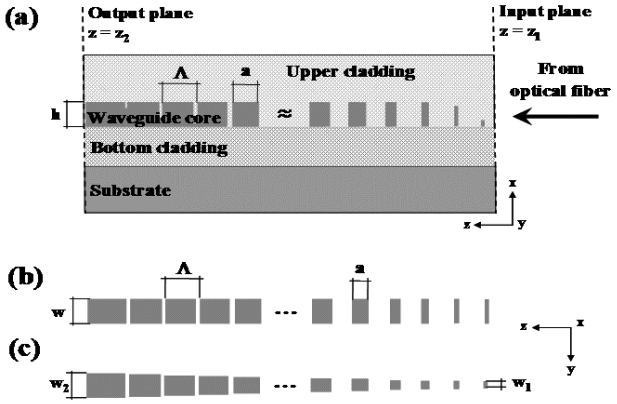

Figure 5. A general schematic of the proposed subwavelength grating coupler. (a) The cross-sectional view; (b) and (c) the top views of the SWG structures whereas (c) combines SWG effect with waveguide width tapering.

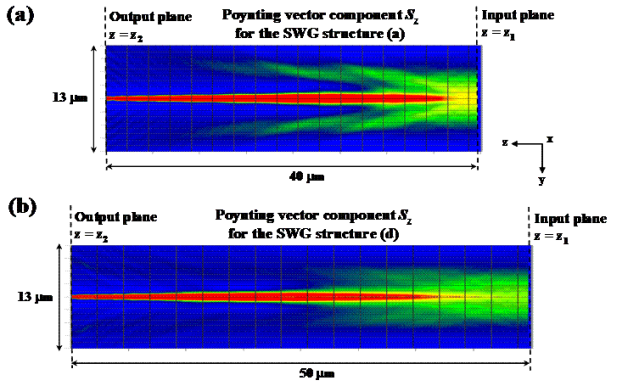

Figure 6. Calculated Poynting vector component $S_z = \mathrm{Re}(E_x H_y^*)/2$ for SWG couplers in the SOI platform. (a) SWG structure without waveguide width tapering, (b) SWG structure with waveguide width tapering. For both structures, Si waveguide thickness is 0.3 μm and input mode field diameter is 10.4 μm, as in SMF-28 fiber.

Fig. 6a shows the Poynting vector component $S_z = \mathrm{Re}(E_x H_y^*)/2$ along the propagation direction (z) obtained for a 2D FDTD calculation of a coupler with an overall length of 40 μm, SWG pitch of 0.2 μm, and the duty ratio r linearly chirped from 0.1 to 1. The calculated coupling efficiency is 73.3%, which corresponds to a coupling loss of 1.35 dB. In Fig. 6a it is observed that the loss is primarily incurred along the first 10 μm of the coupler length. To ease the transition, SWG effect can be combined with waveguide width tapering, as schematically shown in Fig. 5c. We calculated several linearly tapered structures and found the coupler efficiency as high as 76% (1.19

dB loss) with SMF-28 fiber, with simulated Poynting vector component S_z shown in Fig. 6b. We found that only 0.03% of power is reflected by the SWG, yielding a negligible return loss of -35 dB. For a high-NA fiber with MFD = 5.9 μm, the calculated efficiency for this structure was 81.4% (0.89 dB loss). Further loss reduction can be expected by a judicious design, including parabolic rather then linear tapering of waveguide width or chirping the SWG pitch. We also observed that an increase in the SWG pitch Λ from 0.2 μm to 0.3 μm results in a negligible excess loss of 0.03 dB. Detailed design and comparison of different SWG coupling structures will be reported.

The results were obtained for light with the electric field parallel to the simulation plane shown in Figure 6. Because these 2D SWG structures are invariant (strips of infinite length) in direction orthogonal to the simulation plane with obviously no sub-wavelength segmentation effect existing in that direction, the 2D structures are not effective for electric field polarized along that direction. At this point we do not have computational tools capable of 3D FDTD simulations of these SWG coupling structures.

We also calculated coupling tolerances to transverse and angular fiber misalignment for coupling from standard SMF-28 fiber. We found that transverse misalignment of ±2 μm (along *y* axis, Fig. 6) results in an increased coupling loss of only 0.5 dB. The angular misalignment tolerance is also large, with only 0.24 dB loss penalty for angular misalignment of ±2 degrees.

We have also investigated the reduction of the coupler length down to 10 μm and found an excess loss of ~ 0.6 dB compared to a 50 μm long coupler. In this calculation we included the height tapering due to aspect ratio dependent etching, or etch lag, that manifests itself as a variation in depth or height of an etched feature proportional to its width.

6 Planar waveguide facets with subwavelength gratings

The functionality and performance of many planar waveguide devices, including lasers and optical amplifiers, are critically affected by the reflectivity of the waveguide facets. For high index contrast waveguide devices, the Fresnel reflection at the facet is a significant contribution to the fibre-to-chip coupling loss and the return loss. Currently, the common method to control the facet reflectivity of planar waveguides is the deposition of anti- or high-reflective coatings.

Schmid et al. have recently proposed the use of SWGs etched into the facets of planar waveguides as an effective means to control facet reflectivity over a wide range of values[11]. To demonstrate the effect we have carried out Finite-Difference Time Domain (FDTD) simulations as well as experiments on silicon-on-insulator (SOI) waveguides for SWGs with triangular and square shaped teeth. Figure 7a shows a scanning electron microscope image of the facet of a 4 μm wide SOI ridge waveguide, with a Si thickness of 1.5 μm, patterned with a triangular SWG with 400 nm pitch and 700 nm modulation depth. The structure was fabricated by a two-step process using electron beam lithography and dry-etching.

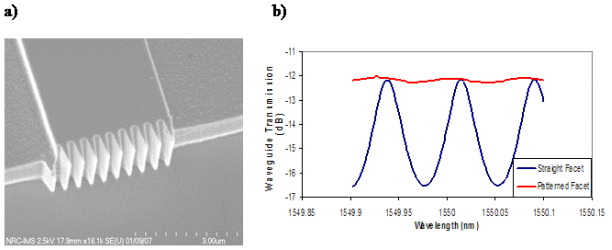

Figure 7. a) SEM micrograph of a SOI ridge waveguide facet patterned with a triangular subwavelength grating. b) Fabry-Pérot fringes in the transmission spectra of waveguides with patterned and unpatterned facets.

The triangular SWG acts as a graded-index (GRIN) boundary, hence reflections are suppressed. Our 2D-FDTD simulations show that the reflectivity of the facets with triangular gratings are 0.2% and 2% for the fundamental TE and TM modes, respectively, for a grating modulation depth of 2 μm. Experimentally, facet reflectivity was estimated from the measurement of Fabry-Pérot (FP) fringes in the waveguide transmission spectrum near λ = 1.55 μm. Figure 7b shows the measured TE transmission spectra of waveguides with unpatterned facets compared to a triangular SWG facet as shown in Fig. 7a. From the measured depth of the FP fringes facet reflectivities as low as 2.0% for TE and 2.4% for TM have been obtained. In contrast to triangular SWGs limited to the anti-reflective effect, with square SWGs, the change in reflectivity is caused by an interference effect depending on the relative amplitudes and phases of the light at the peaks and troughs of the grating and can thus be adjusted arbitrarily. Our FDTD calculations show that by varying the grating pitch, duty cycle and the modulation depth, it is possible to obtain SOI facet reflectivities in a remarkably broad range of ~ 0.2% to 99%.

7 Conclusions

We have reviewed our progress in the development of silicon microphotonic waveguide devices. The results obtained in our compact 50-channel SOI AWG spectrometer suggest that high-resolution spectroscopic applications may be performed at the chip level in the foreseeable future. The Fourier-transform Michelson-type AWG, has an advantage of large device light gathering capability, and as such it can be relevant for spectral analysis of light from diffuse and non-collimated sources, and for improving the spectrometer light gathering capability particularly when the light sources are weak, such as in Raman spectroscopy. We have also discussed a method for mode transformation and light coupling between an optical fiber and a high index contrast waveguide with

sub-micrometer dimensions using a sub-wavelength grating. The proposed principle of effective index modification by SWG effect can also be applied to engineer waveguide properties by SWG-induced effects, including reflectivity control of waveguide facets.

Acknowledgements

This work was supported in part by the Genome and Health Initiative of the National Research Council of Canada.

References

1. P. Cheben, "Wavelength dispersive planar waveguide devices: echelle gratings and arrayed waveguide gratings," in *Optical Waveguides: from Theory to Applied Technologies,* M. L. Calvo and V. Lakshminarayanan, Eds. (CRC Press, London, 2007), Chap. 5.

2. P. Cheben, A. Bogdanov, A. Delâge, S. Janz, B. Lamontagne, M. J. Picard, E. Post, and D-X. Xu, A 100-channel near-infrared SOI waveguide microspectromer: Design and fabrication challenges, in *Optoelectronics Devices and Integration*, SPIE Proc. 5644, 103 (2005).

3. P. Cheben, J.H. Schmid, A. Delâge, A. Densmore, S. Janz, B. Lamontagne, J. Lapointe, E. Post, P. Waldron, and D.-X. Xu, A high-resolution silicon-on-insulator arrayed waveguide grating microspectrometer with sub-micrometer aperture waveguides, Optics Express, 15, 2299 (2007).

4. K. Takada, M. Abe, T. Shibata, and K. Okamoto, Tandem multi/ demultiplexer covering the S-, C-, and L-bands using arrayed waveguide grating with Gaussian passband as primary filter, IEEE Photon. Technol. Lett. 14, 648 (2002).

5. P. Cheben, I. Powell, S. Janz, and D.-X. Xu, Wavelength-dispersive device based on a Fourier-transform Michelson-type arrayed waveguide grating, Optics Letters 30, 1824 (2005).

6. O. Martínez, M.L. Calvo, P. Cheben, S. Janz, J.A. Rodrigo, D.-X. Xu, and A. Delâge, Arrayed waveguide grating based on group index modification, Journal of Lightwave Technology 24, 1551 (2006).

7. Y.A. Vlasov, M. O'Boyle, H.F. Hamann, and S.J. McNab, Active control of slow light on a chip with photonic crystal waveguides, Nature 438, 65 (2005).

8. M. Notomi, K. Yamada, A. Shinya, J. Takahashi, C. Takahashi, and I. Yokohama, Extremely large group-velocity dispersion of line-defect waveguides in photonic crystal slab, Phys. Review Lett. 87, 253902-1 (2001).

9. P. Cheben, D.-X. Xu, S. Janz, and A. Densmore, Subwavelength waveguide grating for mode conversion and light coupling in integrated optics, Optics Express, 14, 4695 (2006).

10. Z. Weissman and A. Hardy, 2-D mode tapering via tapered channel waveguide segmentation, Electron. Lett. 28, 1514 (1992).

11. J.H. Schmid, P. Cheben, S. Janz, J. Lapointe, E. Post, A. Delâge, A. Densmore, B. Lamontagne, P. Waldron, D.-X. Xu, Photonics North Conference, Ottawa, June 4-7, (2007).